A GEOPHYSICAL STUDY OF THE OPHIOLITE COMPLEX AND THE SEDIMENTARY BASINS IN THE NORTHWEST PART OF THE CHALKIDIKI PENINSULA (N. GREECE)

A.S. SAVVAIDIS, G.N. TSOKAS, C.B. PAPAZACHOS and D. KONDOPOULOU
Geophysical Laboratory, Aristotle University of Thessaloniki, Thessaloniki, Greece

(Received 15 July, 1999; Accepted 7 July, 2000)

Abstract. The present work focuses on the study of the main ophiolite complex of Northern Greece, which is one of the dominant geological features in the broader Aegean area, by the use of geophysical (gravity and magnetic) data. This ophiolite complex, which trends in a NW-SE direction, starts at the eastern part of the borders of Greece with F.Y.R.O.M. and continues up to the southern part of the Chalkidiki Peninsula. The ophiolites mainly consist of dense, high-susceptibility peridotitic and gabbroic rocks. As a result, the southwestern part of the ophiolitic complex, which crosses the northwestern part of the Chalkidiki-Peninsula, gives rise to both high amplitude aeromagnetic and Bouguer anomaly values. On the other hand, the Axios-Thermaikos basin, which is situated at the western border of the ophiolitic complex, exhibits a deep sedimentary cover that results in low Bouguer anomaly values. The corresponding Bouguer anomaly decreases to the southwest, indicating an increase of the sedimentary layer thickness in that direction.

2.5-D inversion was applied to both the aeromagnetic and the Bouguer gravity data along several profiles. All the profiles were oriented normal to the main trend of the ophiolitic complex. Information from two deep boreholes, as well as the surface occurrence of the ophiolites was used as constrains to the inversion scheme. The produced model shows an average sedimentary thickness of 2.5 km along the coastline. From the joint inversion of the Bouguer and aeromagnetic anomaly data the existence of two ophiolitic stripes is revealed. The first "external" one is located in the southwest part, while the other "internal" one to the northeast part of the belt. In the internal one, the depth extent of the ophiolites was estimated to range between 1 to 4 km. Moreover, the ophiolites were found to dip towards the northeast, but their dip varies from 20–45° in the northern part to 10–15° in the southern part of the stripe. For the "external" stripe the extent of the ophiolitic bodies varies from northwest to southeast, reaching its highest depth of 5 km to the south. This stripe is also dipping towards the northeast with a dip of 10–15°.

Keywords: Ophiolites, N. Greece, Gravity, Magnetics, Joint Inversion

1. Introduction

Greece and the broader Aegean area exhibits the highest deformation rate in the whole Africa-Eurasia collision zone (Jackson and McKenzie, 1988). This intense deformation is seen today, as more than 60% of the European seismicity is released in this area (Papazachos, 1990), but is also identified in the past as it has resulted in a complex geological setting for the whole Aegean area. Two of the most dominant features of this geological setting are the internal (IRO) and external (ERO) ophiolite complexes (Mountrakis, 1985). The internal one (IRO) is located in Central

Surveys in Geophysics **21:** 567–595, 2000.

Macedonia (N. Greece) and strikes in a NW–SE direction. The largest part of its surface exposure is located in the Northwestern Chalkidiki area (Figure 1).

The presence of the ophiolites and deep-sea Mesozoic sediments in this section of the Chalkidiki Peninsula suggests that this area was part of a deep sea floor (Tethys?) (Mountrakis, 1990). These formations were obducted from the deep sea floor into their present position during the Late Jurassic. An up to date geotectonic study of the area is presented by Tranos et al. (1999), which gives a depth extent for the ophiolites between 2–3 km, and a thickness less then 2 km. The geological formations have been subjected into a younger transpressional deformation that caused the thrusting observed today. The geotectonic status beholden today is formed of thrusts of two common hanging-wall/footwall geometrical cases. In the first case, both the footwall and the hanging wall rocks dip to the NE with almost similar, but higher (commonly with 50–70° towards NE) angles than the thrust, which dips 10–30° towards NE. The other case refers to a low-angle NE-dipping thrust forming footwall ramp and hanging wall flat geometry.

The first geophysical investigation concerning the subsurface distribution of the ophiolites is that of Makris and Moller (1977), which used seismic, gravity and magnetic data to map the subsurface distribution of the ophiolites and concluded that the ophiolites reach the depth of 2.5 km below sea level. Philipopoulos (1983) presented 2-D models of the ophiolite complex based on aeromagnetic data. In a 2-D model at the area of Triadi (Figure 1) Philipopoulos states that the depth extent of the ophiolites is 1.5 km, having a dip equal to 80° to the northeast at the southwest side of the body and equal to 10–15° to the northeast at the northeast side of the body. South of Triadi, at the area of Vavdos, he estimated that the depth of ophiolites increases to approximately 3 km, having a dip equal to 85–90° to the northeast at the southwest side and a dip of 20–30° to the northeast at the northeast side of the body. Kiriakidis (1984) used gravity and aeromagnetic data to model the ophiolites. He constructed 2-D models along two profiles in the areas of Triadi and Vavdos and estimated that the depth of the ophiolites is 2 km in the area of Triadi and 1 km in the area of Vavdos. For the ophiolitic body at the area of Triadi he evaluated a dip of 30° to the northeast at the southwest side of the body and a dip equal to 60–65° to the northeast at the northeast side of the body. Also for the ophiolitic body at the area of Vavdos he calculated a dip of 30° to the northeast at its southwest side and 5–15° to the northeast at the northeast side of the body.

Due to the presence of hydrocarbon deposits in the area of Epanomi (Figure 1) the Greek Public Petroleum Company has carried out detailed exploration in the area. Seismic lines were shot and two boreholes were drilled which were used to interpret the data, particularly the upper Mesozoic (Roussos, 1993). A 3-D model of the top surface of the limestone is also given. Sousounis (1993) used the same seismic and borehole data for the area of Epanomi, to map the “roof” of the granodiorite, which is below the Mesozoic limestone.

The aim of the present study is to use recently developed techniques (Webrig, 1985) of 2.5-D inversion of both gravity (Rasmussen and Pedersen, 1979) and

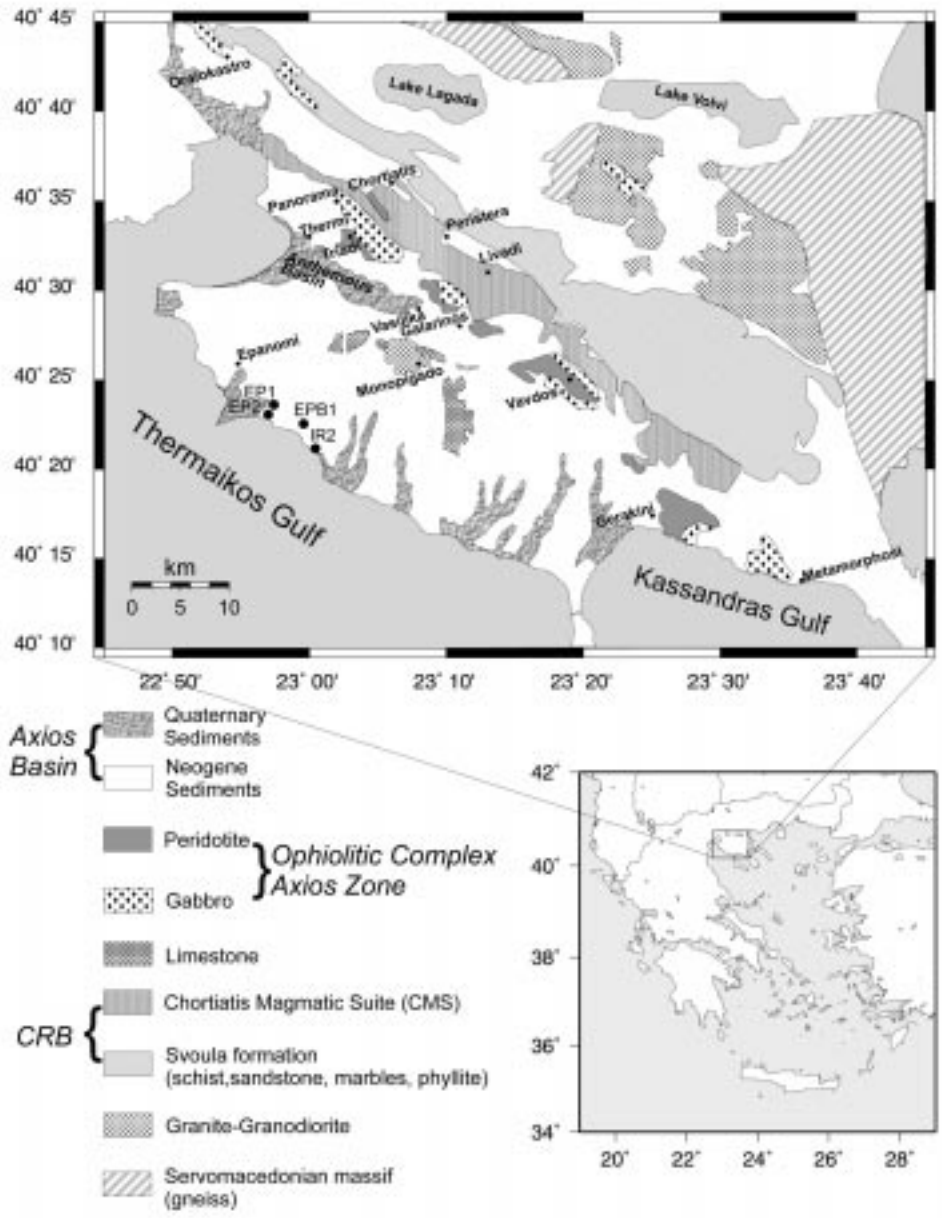

Figure 1. Simplified geological map of the studied area. EP1, EP2, EPB1 and IR2 are the positions of the four deep boreholes in the area. Information from EP1 and IR2 is used in the present study. The Neogene sediments are marked blank in the map. The coastline is given as a solid line.

magnetic data (Shuey and Pasquale, 1973), in order to define the main features of the ophiolite complex and refine earlier models. Moreover, the depth of the sediments in the area of the NW Chalkidiki (Axios Basin) has also been estimated. More further the models estimated are compatible with both the magnetic and the gravity data. Finally, the existence of two ophiolitic stripes is a new result, which is suggested for the first time for the examined area.

2. Geological Setting

The studied area, which is located in Central Macedonia (Figure 1), occupies the inner part of the Hellenic mountain belt including (from the East to West) the Serbomacedonian massif (Sm), the Circum Rhodope Belt (CRB) (as defined by Kauffman et al., 1976) and the Axios zone.

The Sm consists of multiply deformed and metamorphosed Paleozoic or older gneissic rocks that where intruded by Mesozoic and Tertiary acid plutonic rocks (granites and granodiorites, see Figure 1). The CRB comprises Late Paleozoic and Mesozoic marginal sedimentary and volcanic rocks from which in the studied area they form the Chortiatis Magmatic Suite and the Svoula formation. Finally, the Axios zone comprises basic and ultrabasic rocks, representing the ocean (Tethys?) developed in Mesozoic which closed during the Late Jurassic causing the obduction of the ophiolitic rocks onto the carbonate platform (limestones of Up. Jurassic - L. Cretaceous) and the marginal rocks of the CRB (Vergely, 1984).

The rocks of these zones consist of the Pre-Alpine and Alpine basement of the area, which has a NW-SE strike, similar to the general “Dinaric direction” of the Hellenic mountain belt. This “direction” is the result of deformational events associated with the greenschist metamorphism of the area (Mercier, 1968, Tranos et al., 1999) which occurred initially during the Late Jurassic-Lower Cretaceous and mainly during the Late Eocene-Lower Oligocene.

Late Eocene bioclastic limestones and marls as well as Late Eocene-?Early Oligocene sandstones, conglomerates and volcanoclastic rocks rest unconformably on top of the Pre-Alpine and Alpine basement of the area. They form the widely developed molasse-type Axios Trough, as has been well defined by deep boreholes in the area, although they are exposed nowadays in relatively small outcrops. According to Tranos et al. (1999) the aforementioned rocks have been subjected to a younger post-metamorphic transpressional deformation event that caused the thrusting and the repetition of the formations in the area. Finally, a widely extended rift basin, the Axios basin, has developed since the Middle Miocene (Tranos, 1998).

3. Gravity Modeling

3.1. DATA USED

The first gravity anomaly map for the area of Greece has been compiled by Makris and Stavrou (1984) on behalf of the Institute of the Geology and Mining Exploration (IGME). A second attempt was performed by Lagios et al. (1994, 1995, 1996) who collected all the existing gravity data for the broader Aegean area up to 1988. These data were based on the former data set of Makris and Stavrou (1984) but also included data collected in several explorations surveys by the IGME and the former Public Petroleum Company (now Hellenic Petroleum SA.). Data of the Hellenic Military Geographical Service (HMGS) were also included, as well as smaller data sets collected by academic institutions. The Gravity Maps of Morelli et al. (1975a, b) were used for the offshore areas. The final compilation consists of a grid of 1 value every 4-km (Lagios et al., 1995, Lagios et al., 1996), although in some areas the original data distribution is coarser (King, 1998). That grid data, as calculated from the previous mentioned authors, were provided to us in digital form and were used in the present study. It has to be noted here that this compilation is not referenced to IGSN, as has been shown by King (1998).

For the gravity modeling, density values of the main formations were adopted from the work of Kiriakidis (1984) and are based on several rock samples. The average value of 2350 kg/m^3 was assessed to the sediments, and the value of 2923 kg/m^3 to the ophiolites. Roussos (1993) presented the stratigraphic columns of the boreholes EP-1 and EP-2 in the area of Epanomi (Figure 1). According to these results, the Cenozoic sediments have an average thickness of 2600 m at the positions of the two boreholes. However, the thickness of the sediments is equal to 2000 m at the position of borehole IR2 (Figure 1). This information was used to constrain the models in the interpretation of the gravity data. The thickness of the sediments is increasing to the southwest to reach its higher depth, i.e., 8–9 km, at the middle of the basin (Roussos, 1994, Papazachos, 1998). Information presented in Roussos (1994), from borehole data, show a continuous “sinking” of the basin, a transgression and regression of sea to the northeast, comprising a typical basin geometry with a direction of NW–SE reaching its maximum depth in the middle of Thermaikos Gulf (Figure 1).

3.2. DATA PROCESSING

The gravity anomaly map for the study area is presented in Figure 2. A Bouguer anomaly high (50–70 mGal) trending NW–SE can be easily recognized in the study area, which should clearly be attributed to the ophiolitic complex. This stripe has a northwest to southeast direction following the general direction of the Hellenides. The highest values of the elongated anomaly stripe are located very close to the northeastern part of the surface occurrence of the ophiolites (Figure 2). The mean density values of the surface geological formations based on rock samples are:

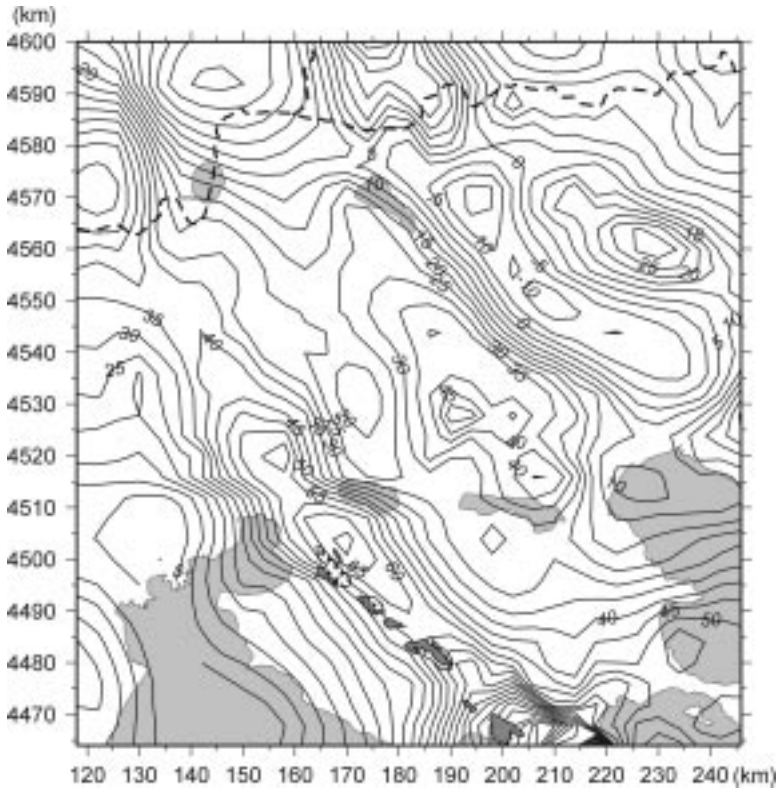

Figure 2. Gravity anomaly map of the broader study area (units are in mGal and the contour level is 5 mGal). The gravity anomaly values are based on the Geodetic Reference Formula of 1967 and were referred to the 1971 International Gravity Standardization Network (IGSN 71). The Bouguer density applied was 2670 kg/m^3. The coastline is denoted with solid line and the national borders with dashed line. The formations of the ophiolitic complex are denoted similarly to Figure 1.

granite 2610 kg/m^3, granodiorite 2610 kg/m^3, sediments 2350 kg/m^3, peridotite 3080 kg/m^3, gabbro 2766 kg/m^3, CMS 2670 kg/m^3, limestone 2690 kg/m^3 and Svoula formation 2610 kg/m^3 (Kiriakidis, 1985). These data have a mean value of 2673 kg/m^3, which is very similar to the Bouguer density value of 2670 kg/m^3 that was also used in the present study as a background density.

In order to remove the regional field a first-degree polynomial was subtracted from the initial gravity anomaly field. The residual field is shown in Figure 3 where the high positive anomalies (20–40 mGal) associated with the ophiolites are clearly recognized. As it is easily seen from the residual field the 0 mGal contour follows the geological boundary between the sediments (low Bouguer anomalies), and the ophiolites (high Bouguer anomalies), which is one of the reasons for selecting a first degree-polynomial for the regional field, although higher order polynomials were also tested. Sousounis (1993) and Rousos (1993, 1994) using borehole and seismic data suggest an elongated basin structure for the geological formations of

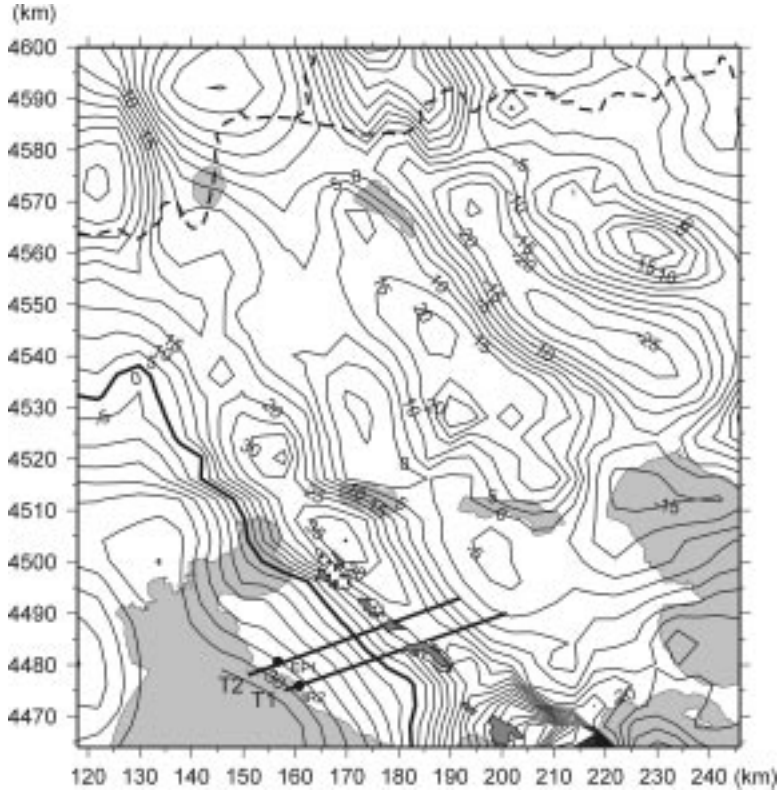

Figure 3. Residual Bouguer map of the studied area after the subtraction of a first order polynomial. The isoanomaly of 0 mGal is marked with a solid line. The two profiles along which 2.5-D modeling was performed are represented by straight solid lines. The formations of the ophiolitic complex are denoted similarly to Figure 1. Units, contour level, datum, type of the IGF and Bouguer density applied are the same with Figure 2.

the area of study with a direction of the axis of the basin NW–SE. Papazachos (1998) using the seismic tomography method show a regional crustal and upper mantle structure with a 2-D geometry elongated along the same direction. This simplified 2-dimensional geometry of the basin and deeper crustal structure, presented in the above-mentioned geophysical-geological reference support the use of a 1st degree polynomial for the regional field modeling. In Figure 3 the locations of the profiles along which 2.5-D modeling was performed are presented. The length of the cross-sections is approximately 45 km and their average direction is ENE–WSW (N70E).

3.3. 2.5-D Modeling

The general pattern of the geological formations and the shape of the Bouguer anomalies mapped imply that a 2.5-D model can adequately depict the ophiolites and the sediments in the area of study. For this reason a 2.5-D inversion algorithm

TABLE I

Information on the density values used in the 2.5 modeling of the gravity data: geological formation, density value, density contrast compared to the background density and reference

Geological formation	Density (kg/m^3)	Den. contrast (kg/m^3)	Reference
Background density (Granodiorite, Limestone, Servomacedonia Basement, ...)	2670	–	Kiriakidis (1984)
Sediments	2350	−320	Kiriakidis (1984)
Peridotite	3080	410	Kiriakidis (1984)
Ophiolites (Gabbro & Peridotite)	2923	253	Kiriakidis (1984)

was applied to the residual field along each of the two profiles. The algorithm is based on the linearization of the nonlinear problem of the dependence of the gravity field with the corresponding source parameters. In our case the source was modeled as a polygonal prism. Using such a linearized method, an algorithm can be developed to determine the best set of prisms for a given anomaly, where the cross-sectional shapes of the prisms are iteratively changed by small amounts through linear least-squares techniques (Corbato, 1965, Johnson, 1969). The computer program of Webrig (1985) that implements the algorithm described (using the algorithms of Rasmussen and Pedersen (1979) for the forward modeling) was used for the inversion in the present study.

Based on the rock sample information, the formations of sediments and the ophiolites were assumed to have discernible density values. The geological formations of granodiorite, limestone and the Servomacedonia basement could not be resolved due to their similar density values. For that reason the background value of 2670 kg/m^3 was used for these formations in the inversion. The values of the densities of the formations that were adopted are shown in Table I. The thickness of the sediments introduced from the well logs of IR2 and EP1 boreholes was used to constrain the inversion for profiles T1 and T2, respectively. Also, the outcrops of the geological formations were adopted as constraints for the polygon shapes.

In Figure 4 the 2.5-D models for both profiles are presented. In the upper part of each sub-figure the observed (triangles) and the calculated (continuous line) values are given. In the lower part the models derived from the inversion scheme are presented. The topography is also given with a solid black line. The position of the boreholes and the thickness of the sediments used as constrain in the inversion, are also shown.

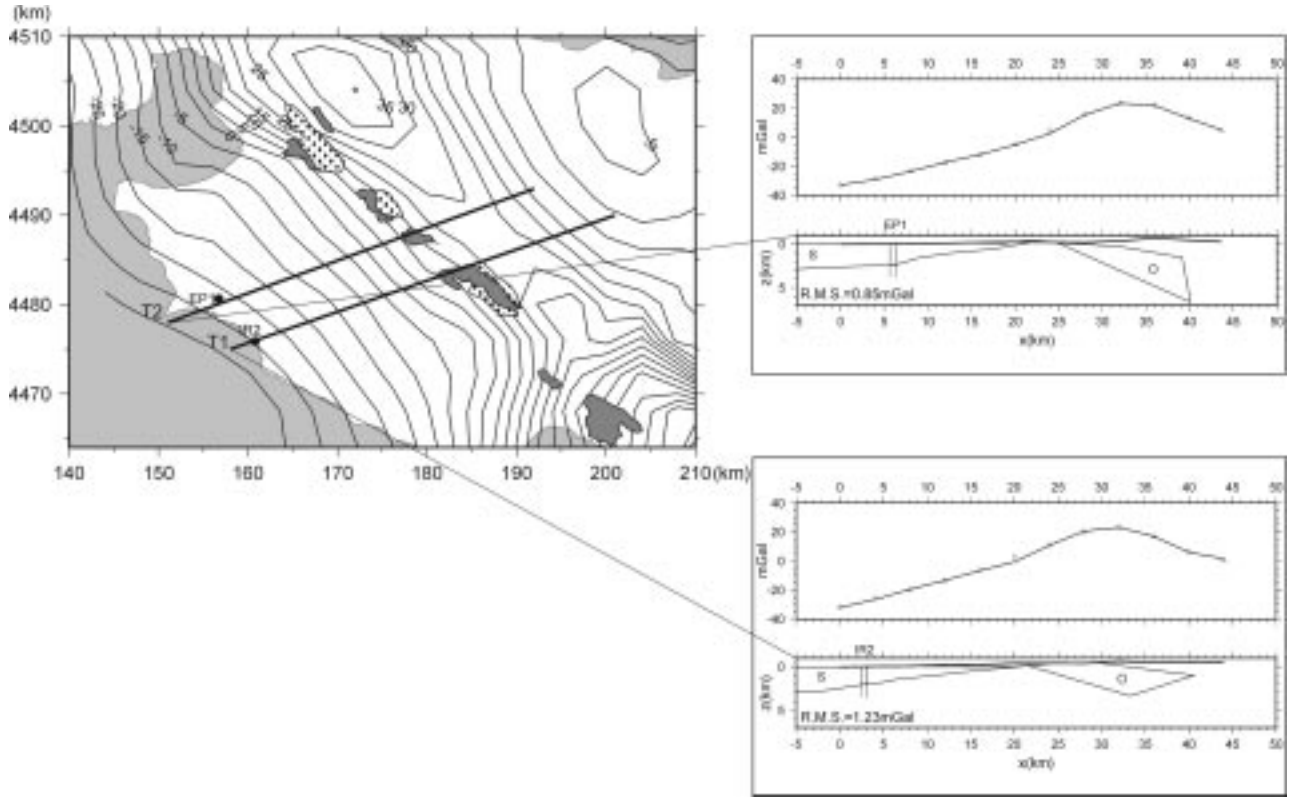

Figure 4. 2.5-D models determined along the cross-sections presented in the left side of the figure. The suggested models are shown in the right side of the Figure in the form of two subfigures, one for each section. In the upper part of each subfigure the observed field is given with triangles and the calculated field is shown with a continuous line. In the lower part of each figure the calculated model is presented (Sediments and Ophiolites). The position of the boreholes from which data were used to constrain the models presented is given in each section. The topography is indicated with a solid black line. Also the R.M.S. misfit value is given for each section.

The models used in the present study are 2.5-D, hence the horizontal dimensions of each model are assumed to be finite in the direction perpendicular to the formation of the cross-section. The lengths were determined on the basis of the gravity anomalies that indicate the spatial extent of the ophiolitic stripe. For example, in the model of cross-section T2 the horizontal size for each body is 40 km towards the southeast and 20 km towards the northwest.

4. Joint Modeling of Gravity and Magnetic Data

4.1. MAGNETIC DATA USED

During 1966 ABEM conducted a large number of aeromagnetic surveys in N. Greece. Recordings of the total magnetic field were performed with flights of stable height (275 ± 75 m) from the surface. The mean distance between the flight lines was 800 m. Four aeromagnetic maps compiled by ABEM (Sheets MACEDONIA 1,2,5,6) which cover the area under investigation, were digitized for the purposes of the present study.

In order to model the maps, measurements of the magnetic susceptibility were also performed using several rock samples from the formations of gabbro, granodiorite, magnesite and limestone. Rock samples were selected from the broader area of Monopigado and Galarinos-Agia Anastasia. Susceptibility measurements were conducted both in the field as well as in the lab, using selected oriented specimens. In all oriented specimens estimation of the magnitude, inclination and declination of the remanent magnetization was also performed. The obtained remanence and susceptibility data for the ophiolites were enriched with available data from the area (Edel personal communication, Philipopoulos, 1983). In Table II the susceptibility and the magnetization data for the ophiolitic complex are presented. The table is sorted by ascending susceptibility order, so that the specimens with the higher susceptibility are grouped at the end of the table. Examination of Table II shows that susceptibility exhibits significant spatial variation, even within the same formation in an examined position. Therefore, this information could not be used to constrain the susceptibility values in the subsequent modeling, since they are varying rapidly in space.

In the fifth column of Table II the intensity of the remanent magnetization for a subset of the specimens presented is shown. The mean magnetization intensity for the gabbro and the peridotite was calculated and compared with the induced magnetization. In general, the remanent magnetization was less than 25% of the induced magnetization for both formations. For this reason, the effect of remanent magnetization was disregarded in the modeling procedure.

TABLE II

Information on the magnetic parameters of the geological formations that comprise the ophiolitic complex: specimen name, site name, geological formation, susceptibility, intensity of magnetization and reference

Specimen	Site	Formation	Susceptibility ($\times 10^{-3}$) EMU	Remanent magnetization (A/m) ($\times 10^{-3}$)	Reference
2G7	Metamorphosi-Gerakini	Gabbro	0,006	1,000	Philipopoulos
1G1	Metamorphosi-Gerakini	Gabbro	0,006	1,000	Philipopoulos
1G2	Vavdos	Gabbro	0,007	5,000	Philipopoulos
1G5	Triadi	Gabbro	0,007	2,000	Philipopoulos
1G10	Panorama	Gabbro	0,008		Philipopoulos
2G4	Vavdos	Gabbro	0,010	1,000	Philipopoulos
2G3		Gabbro	0,010		Philipopoulos
2G5	Metamorphosi-Gerakini	Gabbro	0,012	6,000	Philipopoulos
1G7	Oreokastro	Gabbro	0,014		Philipopoulos
KA30.73	Thermi	Gabbro	0,016		Edel, person. com.
2G9A	Triadi	Gabbro	0,019	70,000	Philipopoulos
1G9		Gabbro	0,020		Philipopoulos
1G6		Gabbro	0,022		Philipopoulos
KA34.23	Thermi	Gabbro	0,023		Edel, person. com.
KA30.22	Thermi	Gabbro	0,023		Edel, person. com.
1G4	Galarinos	Gabbro	0,023	50,000	Philipopoulos
KA37.43	Thermi	Gabbro	0,024		Edel, person. com.
KA31.42	Thermi	Gabbro	0,025		Edel, person. com.
KA37.31	Thermi	Gabbro	0,026		Edel, person. com.
KA30.62	Thermi	Gabbro	0,027		Edel, person. com.
KA31.11	Thermi	Gabbro	0,028		Edel, person. com.
KA42.71	Oreokastro	Gabbro	0,033		Edel, person. com.
KA41.11	Oreokastro	Gabbro	0,034		Edel, person. com.
KA34.33	Thermi	Gabbro	0,034		Edel, person. com.
2G9	Galarinos	Gabbro	0,034	100,000	Philipopoulos
KA41.42	Oreokastro	Gabbro	0,035		Edel, person. com.
KA41.51	Oreokastro	Gabbro	0,036		Edel, person. com.
KA42.43	Oreokastro	Gabbro	0,050		Edel, person. com.
1G12	Vasilika	Gabbro	0,055	50,000	Philipopoulos
KA34.72	Metamorphosi	Gabbro	0,070		Edel, person. com.
KA32.63	Thermi	Gabbro	0,074		Edel, person. com.
2G2	Vavdos	Gabbro	0,091	2,000	Philipopoulos
KA33.53	Gerakini	Gabbro	0,157		Edel, person. com.
KA32.72	Thermi	Gabbro	0,185		Edel, person. com.
2G1	Metamorphosi-Gerakini	Gabbro	0,189	70,000	Philipopoulos
KA33.83	Gerakini	Gabbro	0,226		Edel, person. com.
2G6	Metamorphosi-Gerakini	Gabbro	0,272	140,000	Philipopoulos
KA33.73	Gerakini	Gabbro	0,284		Edel, person. com.
KA33.92	Gerakini	Gabbro	0,436		Edel, person. com.
KA38.33	Thermi	Gabbro	0,455		Edel, person. com.
KA33.63	Gerakini	Gabbro	0,462		Edel, person. com.

TABLE II
Continued

Specimen	Site	Formation	Susceptibility ($\times 10^{-3}$) EMU	Remanent magnetization (A/m) ($\times 10^{-3}$)	Reference
KA33.93	Gerakini	Gabbro	0,516		Edel, person. com.
KA34.02	Metamorphosi	Gabbro	0,550		Edel, person. com.
KA38.43	Thermi	Gabbro	0,811		Edel, person. com.
KA34.83	Metamorphosi	Gabbro	0,904		Edel, person. com.
KA34.92	Metamorphosi	Gabbro	1,020		Edel, person. com.
1G8	Oreokastro	Gabbro	1,226	220,000	Philipopoulos
KA34.12	Metamorphosi	Gabbro	1,301		Edel, person. com.
KA34.13	Metamorphosi	Gabbro	1,357		Edel, person. com.
KA34.23	Metamorphosi	Gabbro	1,461		Edel, person. com.
KA58.83	Gerakini	Gabbro	1,498		Edel, person. com.
KA34.43	Metamorphosi	Gabbro	1,907		Edel, person. com.
KA34.63	Metamorphosi	Gabbro	2,257		Edel, person. com.
KA58.43	Gerakini	Gabbro	4,388		Edel, person. com.
KA38.13	Thermi	Gabbro	4,894		Edel, person. com.
1P2	Metamorphosi-Gerakini	Peridotite	0,004	150,000	Philipopoulos
ANAS1F	AgiaAnastasia	Peridotite	0,006	0,036	This study
ANAS1A	AgiaAnastasia	Peridotite	0,006	0,363	This study
ANAS1E	AgiaAnastasia	Peridotite	0,008	0,178	This study
ANAS1G	AgiaAnastasia	Peridotite	0,009	0,031	This study
ANAS1D	AgiaAnastasia	Peridotite	0,009	0,131	This study
ANAS1B	AgiaAnastasia	Peridotite	0,009	0,398	This study
ANAS1C	AgiaAnastasia	Peridotite	0,010	0,361	This study
3P3	Livadi	Peridotite	0,011		Philipopoulos
1P4	Vavdos	Peridotite	0,013	35,000	Philipopoulos
1P1	Metamorphosi-Gerakini	Peridotite	0,013	50,000	Philipopoulos
2P2	Metamorphosi-Gerakini	Peridotite	0,022	20,000	Philipopoulos
KA59.73	Gerakini	Peridotite	0,041		Edel, person. com.
KA59.53	Gerakini	Peridotite	0,045		Edel, person. com.
2P1	Metamorphosi-Gerakini	Peridotite	0,046	140,000	Philipopoulos
2P6	Vavdos	Peridotite	0,056	27,000	Philipopoulos
1P11		Peridotite	0,059		Philipopoulos
2P4	Vavdos	Peridotite	0,096	52,000	Philipopoulos
2P9	Triadi	Peridotite	0,106	115,000	Philipopoulos
1P6		Peridotite	0,111		Philipopoulos
KA59.22	Gerakini	Peridotite	0,114		Edel, person. com.
KA57.85	Thermi	Peridotite	0,132		Edel, person. com.
KA57.83	Thermi	Peridotite	0,145		Edel, person. com.
KA57.81	Thermi	Peridotite	0,170		Edel, person. com.
2P5	Vavdos	Peridotite	0,217	45,000	Philipopoulos
1P10		Peridotite	0,222		Philipopoulos
2P3	Metamorphosi-Gerakini	Peridotite	0,226	800,000	Philipopoulos

TABLE II
Continued

Specimen	Site	Formation	Susceptibility ($\times 10^{-3}$) EMU	Remanent magnetization (A/m) ($\times 10^{-3}$)	Reference
1P3	Metamorphosi-Gerakini	Peridotite	0,238	200,000	Philipopoulos
1P7	Triadi	Peridotite	0,284	475,000	Philipopoulos
3P1	Peristera	Peridotite	0,756		Philipopoulos
3P2	Peristera	Peridotite	0,780		Philipopoulos
2P8	Galarinos	Peridotite	0,900	115,000	Philipopoulos
1P8	Panorama	Peridotite	1,012		Philipopoulos
KA10.44	Panorama	Peridotite	3,323		Edel, person. com.
KA10.43	Panorama	Peridotite	3,523		Edel, person. com.
KA9.44	Panorama	Peridotite	3,567		Edel, person. com.
KA9.43	Panorama	Peridotite	3,581		Edel, person. com.
3P4	Chortiatis	Peridotite	3,719		Philipopoulos
KA9.54	Panorama	Peridotite	4,107		Edel, person. com.
KA9.51	Panorama	Peridotite	4,408		Edel, person. com.
KA10.21	Panorama	Peridotite	4,501		Edel, person. com.
KA9.65	Panorama	Peridotite	6,317		Edel, person. com.

4.2. DATA PROCESSING

The digitized data were used to calculate a grid with grid spacing of 0.5 km. The newly calculated contours are practically the same, both in position and amplitude with the original contours presented by ABEM. The minimum curvature algorithm was used for the interpolation and the corresponding anomaly map is presented in Figure 5, where contours are shown only for areas were original observations are available (no contours are shown for the southwestern part of the map). It can be easily seen that there is a high anomaly stripe in the studied area, which is attributed to the ophiolitic complex, directed almost Northwest to Southeast (direction of the Hellenides). In general, the stripe is elongated in a direction of 135° (clockwise from North).

The regional magnetic field was modeled with a first-degree polynomial and subtracted from the initial field. The direction of 135° was constrained as the direction parallel to which the regional field was considered to be stable. This direction was selected similarly to the gravity data since it coincides with the main trend of the crustal structure (Papazachos, 1998) and the elongation of the ophiolites, which cause the high amplitude magnetic anomalies, implying that a first degree polynomial can adequately describe the regional field. For this reason two lines parallel to the trend of the ophiolites, given in Figure 5 with letters A and B, were drawn, at a significant distance from the ophiolite outcrops. Since the

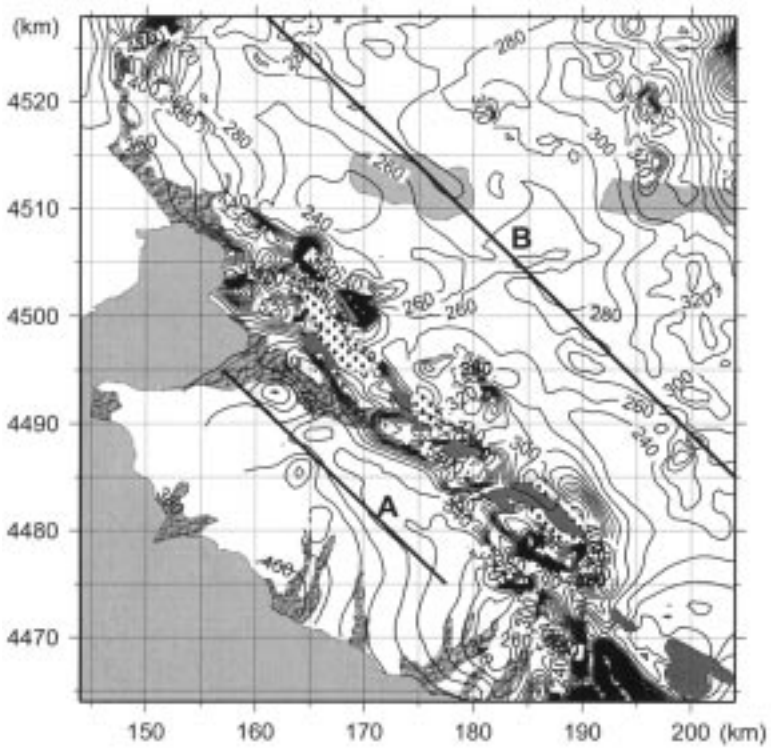

Figure 5. Total aeromagnetic anomaly map used in the present study. Regional correction was based on IGRF of epoch 1965. The values of the magnetic field along the two profiles denoted with letters A and B were used to calculate the parameters of the regional field. The formations of the ophiolite complex are denoted similarly to Figure 1.

regional magnetic field along each line is almost constant, the parameters of a first-degree polynomial function, which describes the regional field were calculated. This procedure was adopted since the spatial extent and strength of the magnetic anomalies due to the ophiolites is quite large and prohibits the use of traditional techniques for regional field removal (filtering, low-order polynomial fit, etc.) The residual field is presented in Figure 6. It can be observed that the adopted procedure for the regional field removal succeeded in exhibiting the high-amplitude (40–550 nT) magnetic anomalies associated with the ophiolites.

4.3. 2.5-D MODELING

As it can be seen in Figure 6, the surface occurrences of the ophiolites, gabbro and peridotite are located within the high aeromagnetic anomaly area. The part of the ophiolitic complex marked with letters A-D mainly consists of both peridotite and gabbro, giving rise to the high magnetic anomaly values. Due to the complicated position of these two formations and for the modeling of the aeromagnetic data,

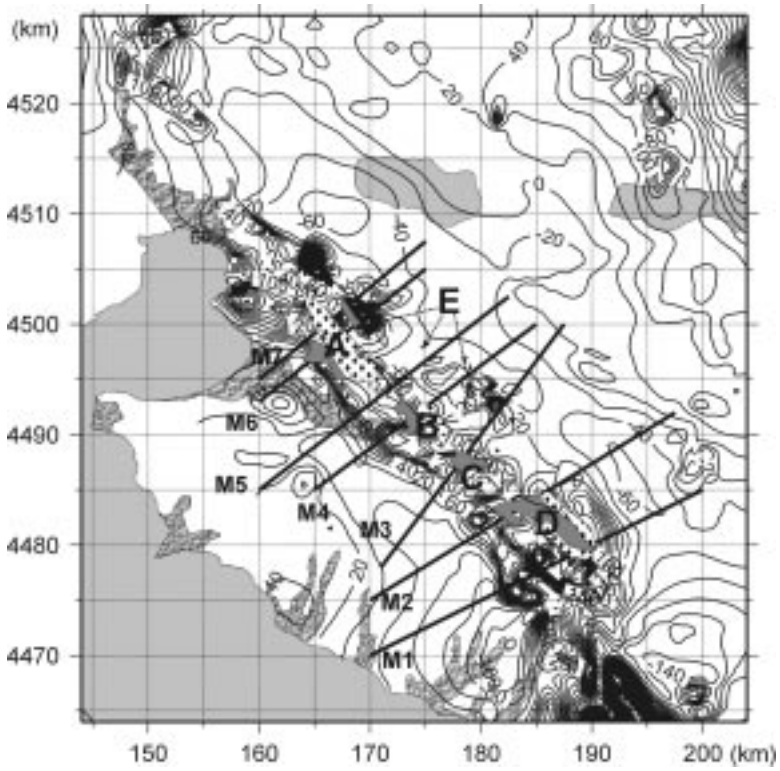

Figure 6. The residual aeromagnetic map of the studied area after the subtraction of a first order surface. The units are in nT and the contour level is 20 nT. The seven profiles along which 2.5-D modeling was performed are represented by straight solid lines. Exposures denoted with letters A-D comprise the main (external) ophiolitic stripe, while exposures denoted with letter E comprise the second (internal) one.

one susceptibility value was used for both gabbro and peridotite for these two geological formations. However, as it can be seen in Figure 6, a second ophiolite body is located northeast of the one described above. The high magnetic anomaly values and small surface occurrences of peridotite define this stripe, which are denoted with letter E in Figure 6. For the modeling of this second stripe of ophiolites the susceptibility value of the peridotite was adopted, as only surface occurrences of peridotite are found in this area. It has to be noted here that these surface occurrences of peridotite can only be identified in geological maps of much higher scale than the ones presented in this study.

2.5-D inversion of the aeromagnetic data was applied along seven profiles. The computer program of Webrig (1985) using the algorithms of Shuey and Pasquale (1973) for the forward modeling was used for the inversion. For the first ophiolitic stripe, the northeast surface occurrences of the ophiolitic bodies were used as constraints in the inversion. This choice was made because the aeromagnetic anomalies extend much more to the southwest, revealing the possible extension of

the ophiolites to that direction. On the northeast side of the ophiolites the Chortiatis magmatic suite is situated, providing a constraint on the surface limit of the ophiolites with the CMS.

Due to the highly varying susceptibility values we decided to preliminary constrain the magnetic models through profiles M1-M7 by calculating first the gravity models for these profiles. After that a joint inversion using both the gravity and magnetic data was introduced, having as an input the models produced from the gravity data modeling. In the joint inversion the susceptibility values were allowed to vary for the different ophiolitic bodies in order to get the best fit for both magnetic and gravity data. The results from the joint inversion are presented in Figure 7. In the middle and upper part of each sub-figure the observed (triangles) and the calculated (continuous line) values are given for the gravity and magnetic field, respectively. In the lower part the model determined from the inversion scheme is given, while the topography is presented with a solid black line. Three types of bodies are shown in Figure 7. The first one is the sediments which dimensions are constrained only from the gravity data. The second one is of ophiolitic origin (gabbro and peridotite) determined from both magnetic and gravity data. The last one is suggested to be of peridotite origin and is also determined from both gravity and magnetic data. In all cases, the horizontal dimensions of the 2.5-D models perpendicular to the cross-section were assumed for each model, similarly to the gravity data. The susceptibilities calculated for the ophiolitic body and the peridotite for each cross-section are presented in Table III, where the name of the cross-section, the geological formation suggested and the susceptibility value calculated are given.

5. Discussion

Quantitative results on the extent of the sediments and the ophiolites in the area from the Bouguer anomaly data are presented in Figure 4. The depth of the sediments reaches the value of 2.5 km at the coastline as this is constrained from borehole data in the area. By the assumption that the ophiolites in the area form a single body, its extent and dip were initially calculated only from the gravity data. A depth extent of 4-6 km and a dip of 20–30° to the NE is suggested. However these results are only based on the Bouguer anomaly data, which have a resolution of a grid value approximately every 4 km, hence they can only give “rough” quantitative results.

The final models determined from the Bouguer anomaly data and the aeromagnetic anomalies are shown in Figure 8. The suggested depth of the sediments follows the results already presented in Figure 4. However an increase in the depth of the sediments is calculated in sections M6 and M7. That is due to the Anthemous Basin (Figure 1) that is located at the SW side of the cross-sections. The existence of two ophiolitic stripes of NW–SE direction is very clearly defined. The external

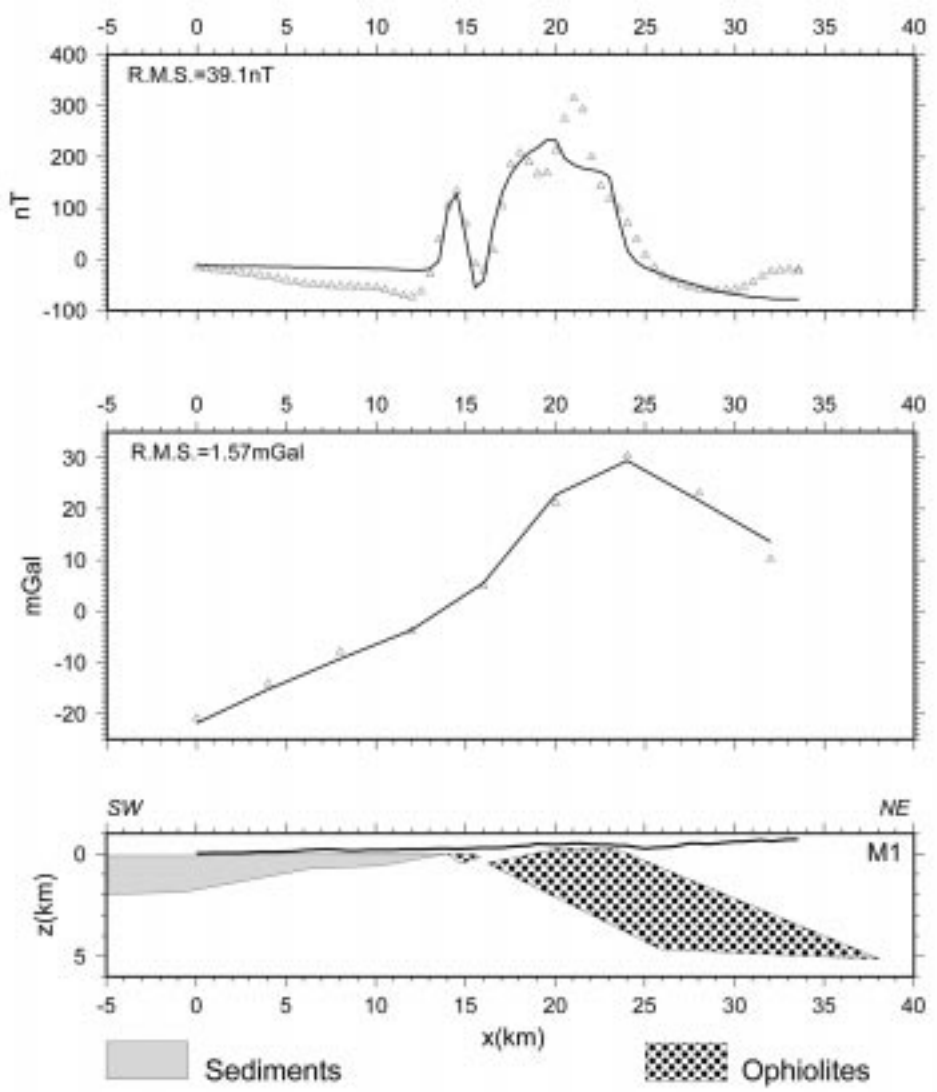

Figure 7. 2.5-D models determined along the cross-sections of Figure 6, (a) M1, (b) M2, (c) M3, (d) M4, (e) M5, (f) M6, (g) M7. In the middle and upper part of each figure the observed field is given with triangles and the calculated field shown with a continuous line for the gravity and magnetic data, respectively. In the lower part of each figure the calculated model is presented. The topography is indicated with a solid black line. Also the R.M.S. misfit value is given for each section.

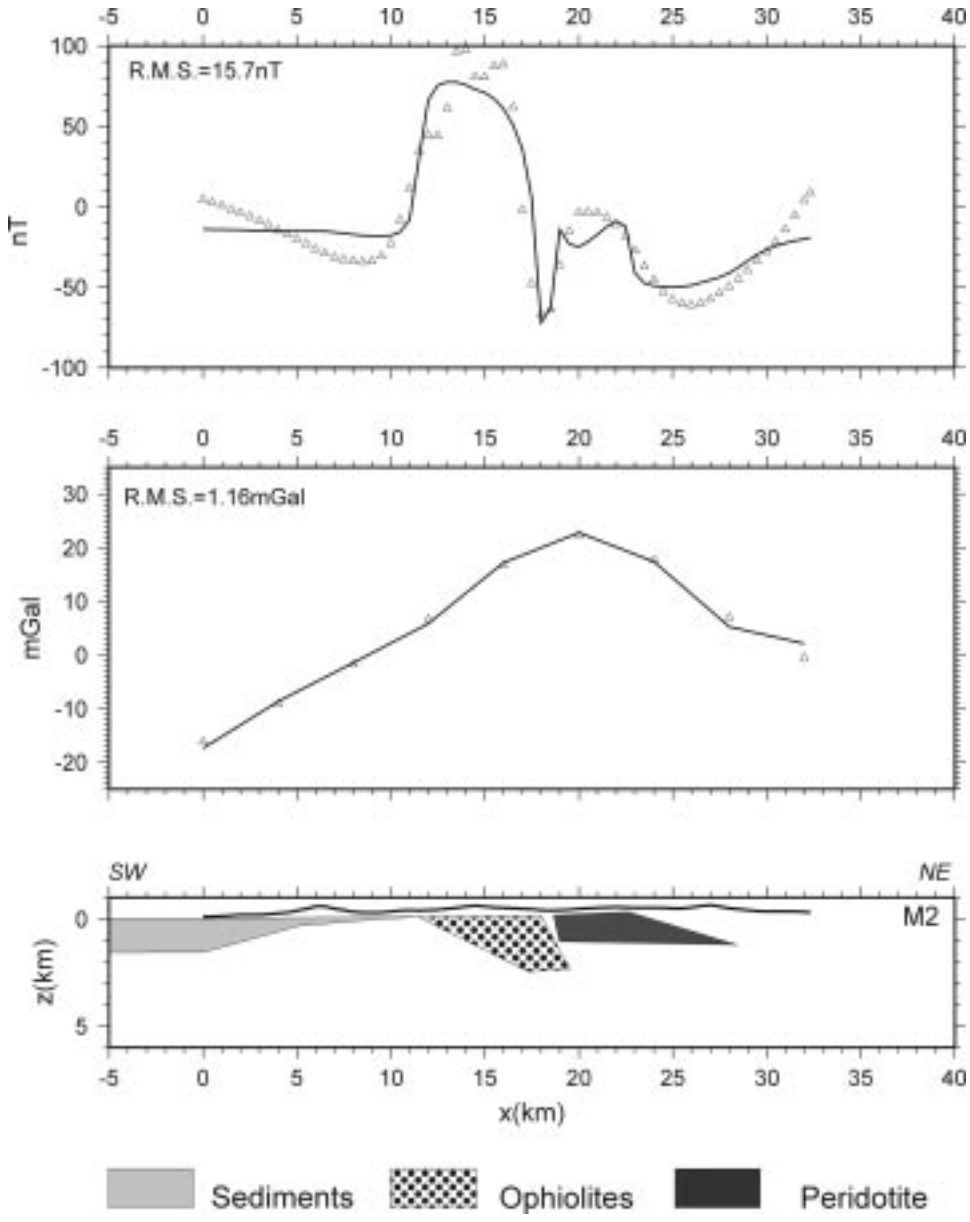

Figure 7b.

one, to the southwest, shows a very good correlation with the surface occurrences (A–D in Figure 8) of the ophiolites and exhibits very well defined bodies. The internal one, to the northeast, is also recognized although it is not clearly identified in the geological maps except for a few surface occurrences at the northern part.

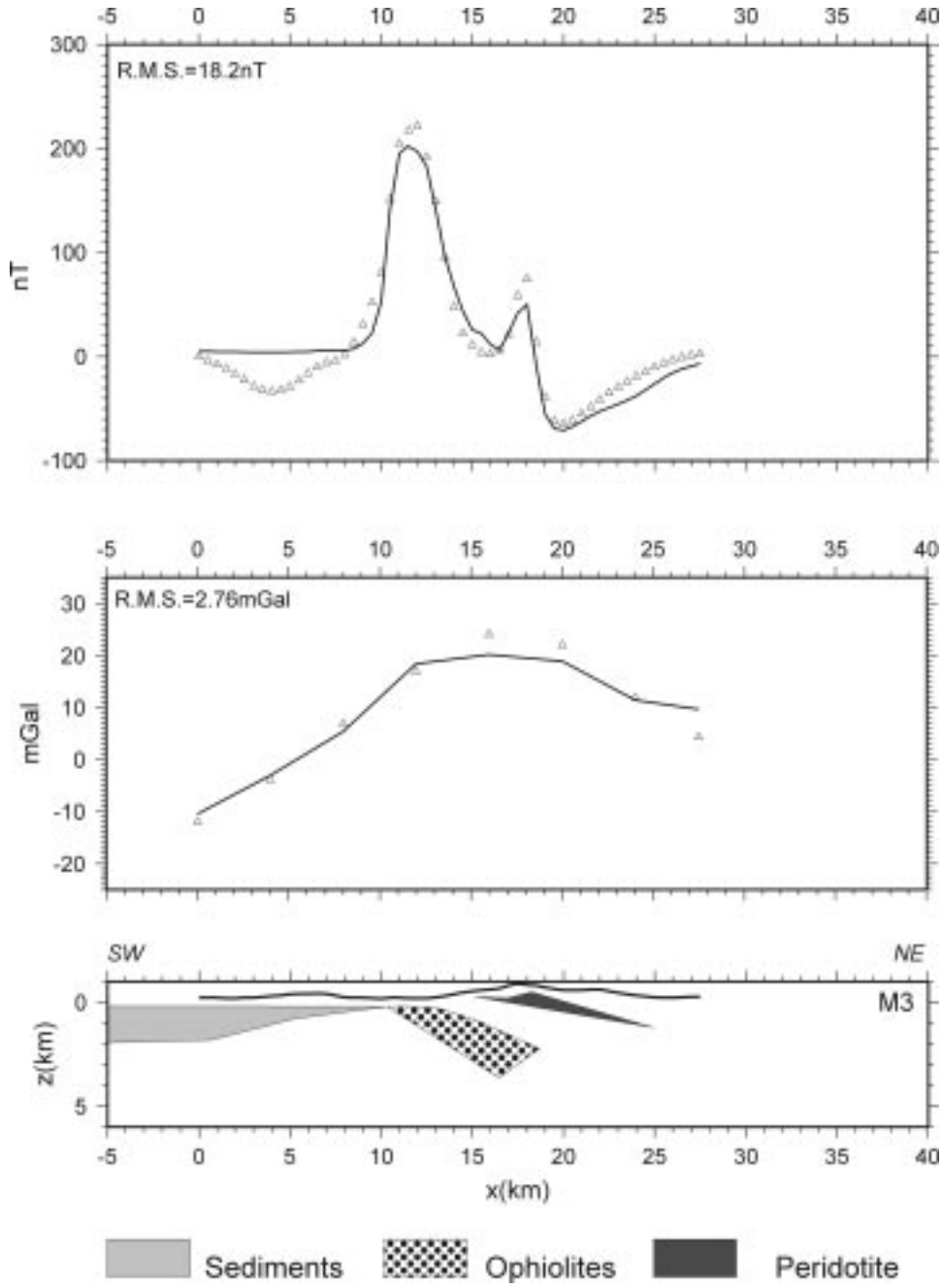
R.M.S.=18.2nT
nT
R.M.S.=2.76mGal
mGal
SW
NE
M3
z(km)
x(km)
Sediments
Ophiolites
Peridotite

Figure 7c.

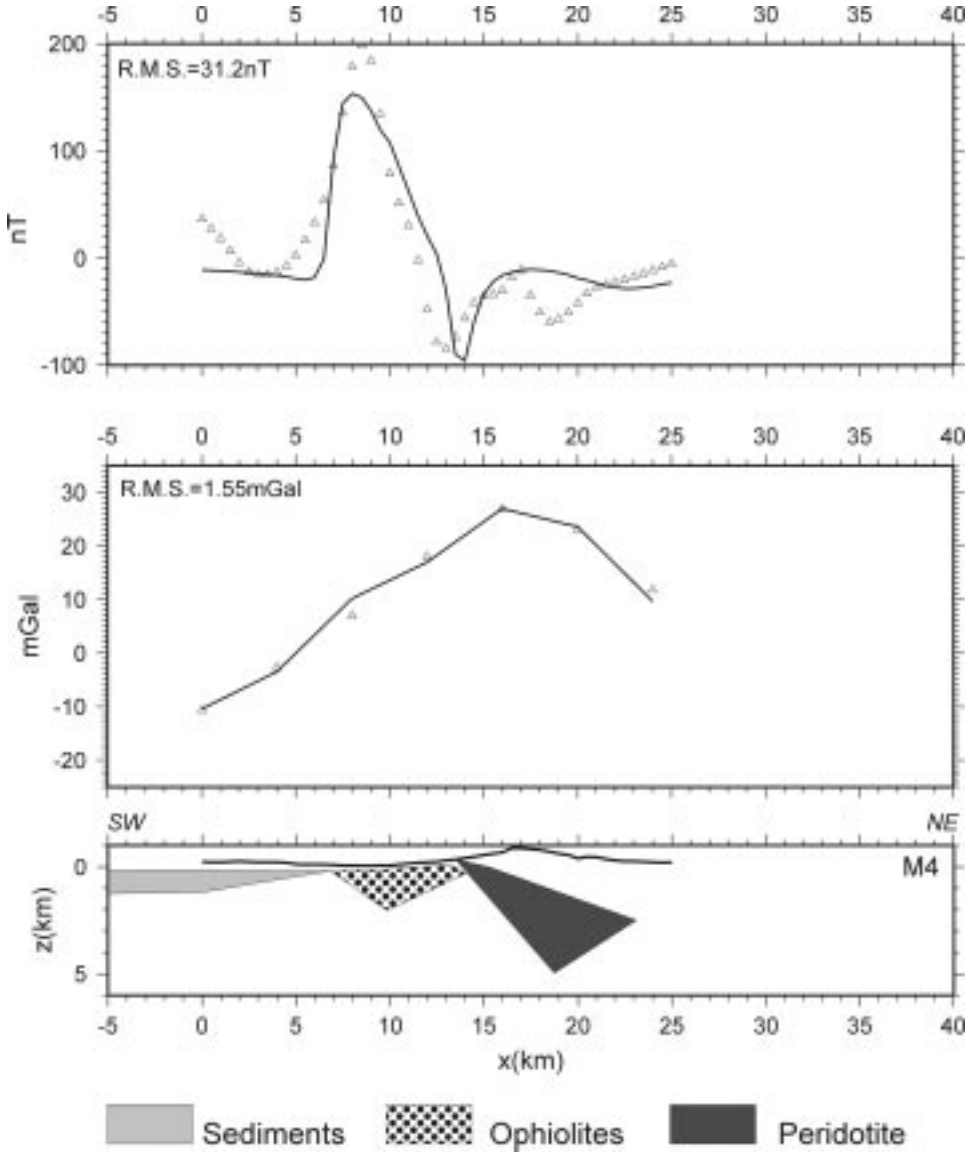

Figure 7d.

This internal stripe mainly consists of peridotite (E in Figure 8) and results in high aeromagnetic anomalies mostly in the northern part.

The external ophiolitic stripe has a dip around 15–40° with a mean thickness of 1.25 km. Also, its depth varies between 1 and 3 km for the majority of the bodies except from the ophiolitic exposure south from the area of Vavdos (D in Figure 8) where it reaches a maximum depth of 5 km.

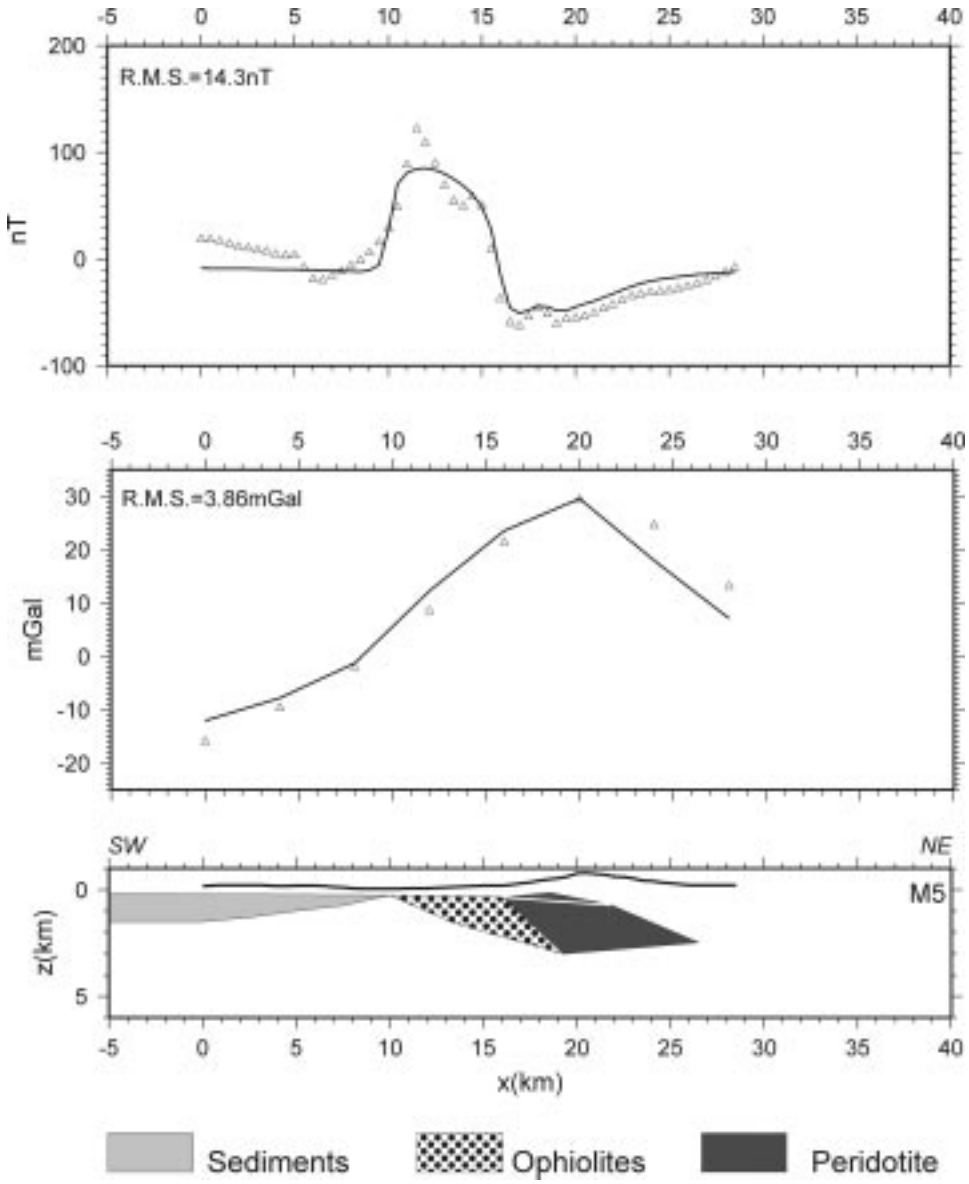

Figure 7e.

The major peridotite bodies (cross sections M4–M7) define the internal ophiolitic stripe with a dip of 20–45° and a depth between 2.5 and 4 km. The extent of the peridotite bodies to the south (cross sections M2–M3) is decreasing to a depth of 1–1.5 km with a dip between 10–15°. Finally at cross section M1 the internal ophiolitic stripe does not appear either in the geological map or in the aeromagnetic anomaly map.

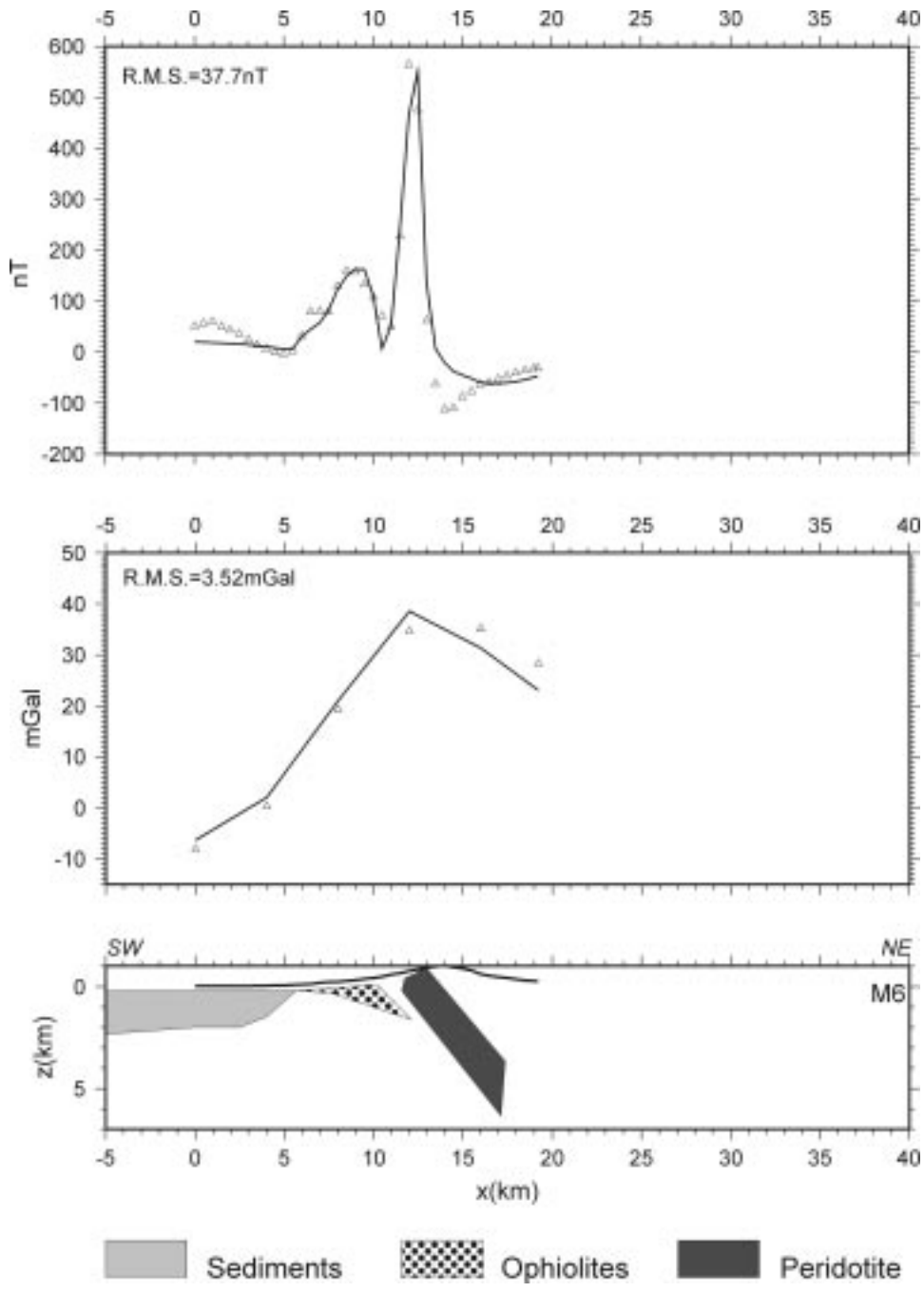
R.M.S.=37.7nT
nT
R.M.S.=3.52mGal
mGal
SW
NE
M6
z(km)
x(km)
Sediments
Ophiolites
Peridotite

Figure 7f.

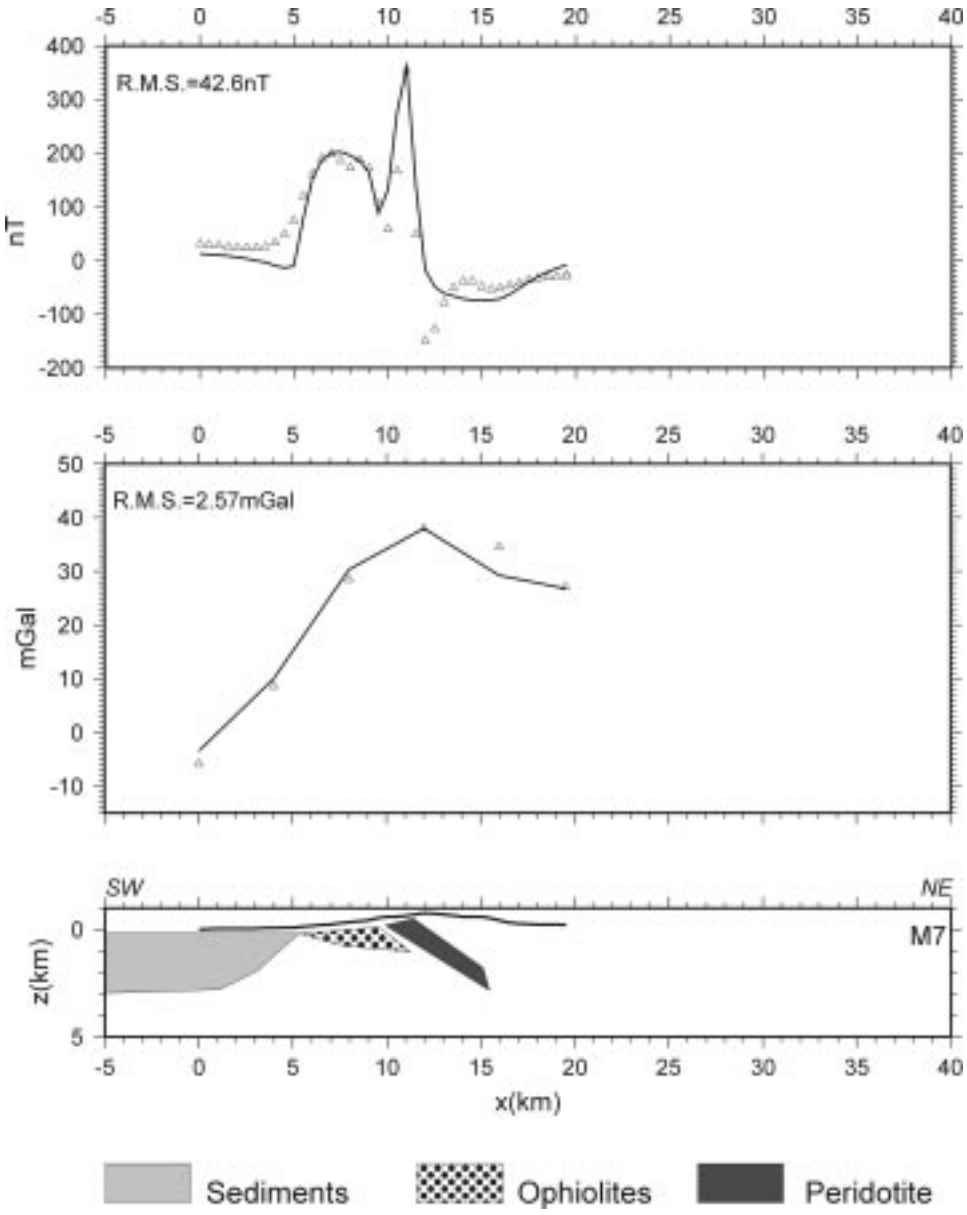

Figure 7g.

In general, the previous results of Makris and Moller (1977), Philipopoulos (1983), and Kirikiadis (1984) are in good agreement with the present study concerning the direction, the extent of the ophiolites and approximately their dip angle values, as well as their depth. In particular, the depth extent of the ophiolites in the area of Triadi presented in Makris and Moller (1977), Philipoulos (1983) and

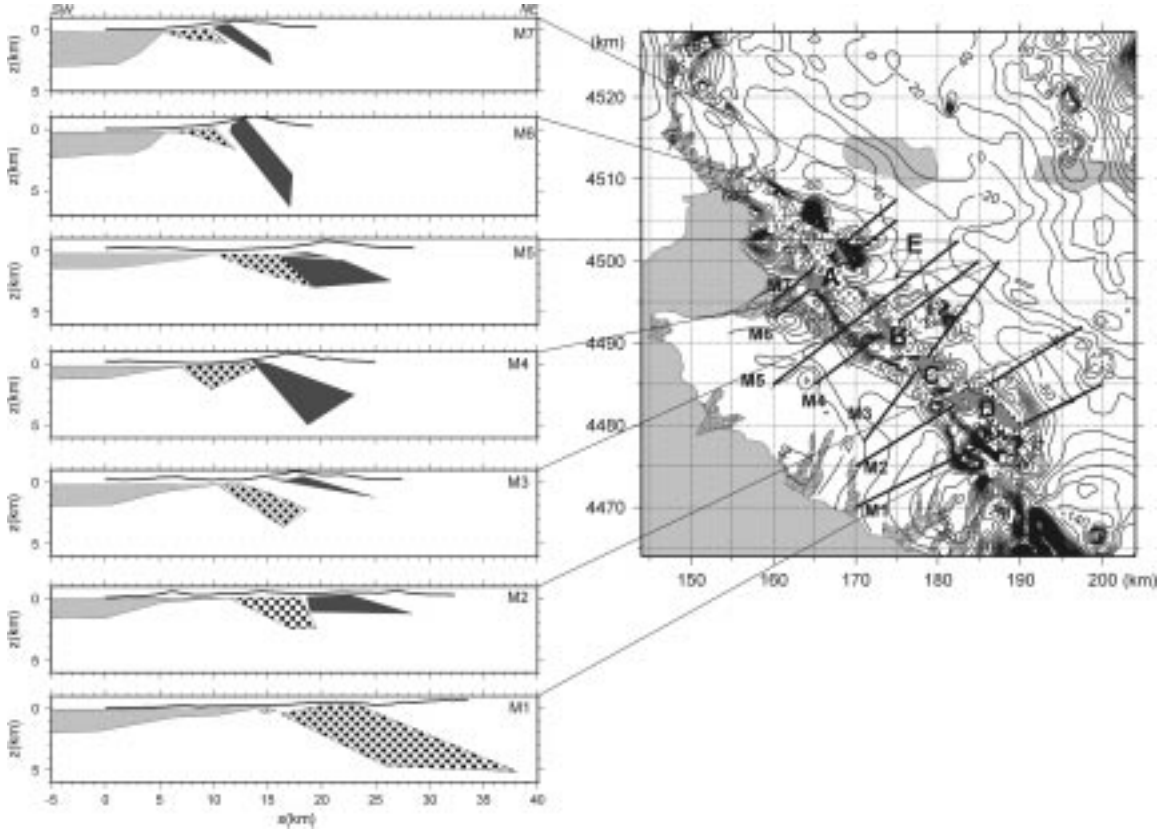

Figure 8. Final 2.5-D models constructed from the gravity and aeromagnetic data. The residual aeromagnetic anomaly map (Figure 6) is shown at the right part of the figure. Straight solid lines present the positions of the seven profiles.

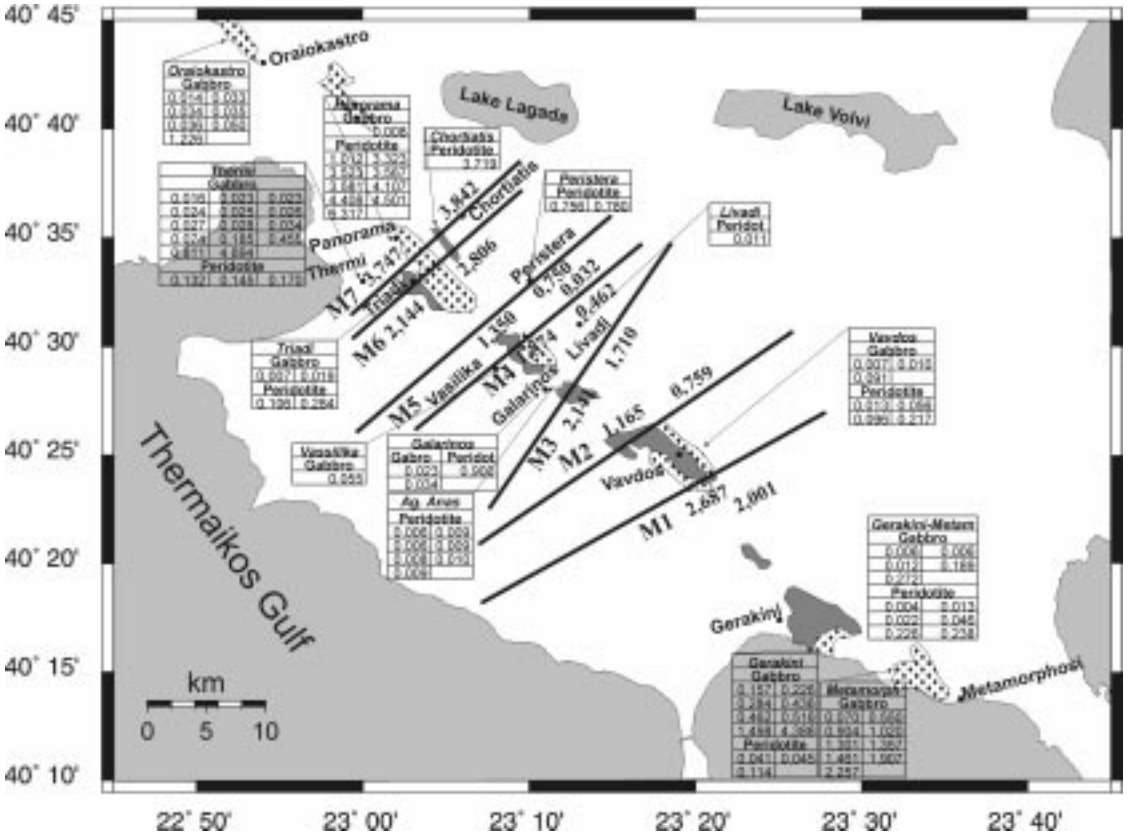

Figure 9. Map of the spatial distribution of the susceptibility values, as this is determined from reference data. For each area a table is presented with the name of the area at the top, the geological formation for which data exist and the corresponding susceptibility values. Also the susceptibility values calculated for each profile from the modeling are given along the solid black lines that show the positions of the seven profiles.

TABLE III

Susceptibilities values suggested for the ophiolites from the modeling of the magnetic data: name of the cross-section, geological formation and susceptibility value

Cross section	Geological formation	Susceptibility ($\times 10^{-3}$) EMU
M1	Ophiolite (Shallow)	2,687
	Ophiolite (Deep)	2,001
M2	Ophiolite	1,165
	Peridotite	0,759
M3	Ophiolite	2,141
	Peridotite	1,710
M4	Ophiolite	1,874
	Peridotite	0,462
M5	Ophiolite	1,350
	Peridotite (Shallow)	0,750
	Peridotite (Deep)	0,032
M6	Ophiolite	2,144
	Peridotite	2,806
M7	Ophiolite	3,747
	Peridotite	3,842

Kiriakidis (1984) is in agreement with the present study, which indicates a value between 1 to 3 km. The dip angle of the ophiolites that are proposed in this study, for the same area are 15–40°, values which are smaller than the dip angle proposed by Kiriakidis (1984) that is varying from 30° to 65°.

The independent results of Tranos et al. (1999) based on geotectonic information are in agreement with the present study concerning the maximum depth of the ophiolites, which varies between 2–3 km. Also the dip angles presented from Tranos et al. (1999) for the thrusts that describe the geotectonic position of the ophiolites correspond well with the results obtained in the present work. This is especially valid for the mean angles of 22.5° and 50° that are calculated for the hanging wall and the footwall, respectively, of the peridotite bodies presented in Figure 8. These results confirm the thrusting faults that have positioned the ophiolites in their present position and are responsible for their geometry. The main difference of the present study, compared to previous results, is the modeling procedure and identification of two, rather than one, ophiolitic stripes. The internal one is defined by peridotite bodies and the external one is represented with both gabbro and peridotite.

The R.M.S. error between observed and computed values is lower than 4 mGal for all models based on the Bouguer anomaly data. Also, for the modeling of the

aeromagnetic data the fit between the response of the determined models and the observed magnetic anomaly values is quite good, with RMS values around 10–40 nT. These relative low RMS misfit values obtained through a joint inversion and the quality of the fit between observed and modeled data (Figure 7) suggest that the obtained models are quite robust.

The spatial distribution of the susceptibility values reported from different authors is presented in Figure 9. For each area that reference data exist, a table with the susceptibility values is given. Susceptibility values are in SI units ($\times 10^{-3}$). It is obvious that the susceptibility values do not show any specific distribution except from the very high values in the areas of Panorama and Chortiati at the north part of the area of study and some high values at the south part in the areas of Gerakini and Metamorphosi. In the same figure the susceptibility values calculated through the inversion are presented along each cross-section as these are listed in Table III. As it is easily seen there is a similar variation for the susceptibilities calculated to the one described above from information based on reference data, as the highest values have been determined for the area of Chortiatis and Panorama for both the peridotite and the gabbro. Also high susceptibility values are also found for the south part of the area of Vavdos, similarly to the measured susceptibility data.

An indirect implication of the suggested model could be mentioned in relation to the paleomagnetic study in the area (Edel et al., 1991/1992). The oldest (Mesozoic) overprint detected in this ophiolite complex displayed a declination of about 310° and approximately 20° inclination. This direction could not be accurately tilt-corrected due to the absence of palaeohorizontal indicators. The dip of the ophiolite bodies (20–40°) suggested here allows such a correction, with no major change in the declination value. As a result the suggested reconstruction of the geological history is more valid.

6. Conclusion

The ophiolite masses in the northwest part of the Chalkidiki Peninsula give rise to high gravity and aeromagnetic anomalies, along the NW–SE direction of this formation. From gravity data, the sedimentary layer thickness in the area increases to the southwest, reaching the value of 2.5 km near the coastline. The gravity models suggest that the ophiolitic complex dips towards the northeast. This is confirmed by the aeromagnetic data, which also reveal the existence of two separate ophiolitic stripes. A joint inversion of the Bouguer anomaly and the aeromagnetic data was used to model these two ophiolitic stripes. The external one, to the southwest, exhibits a dip of the order of 20–30° and depth extent ranging between 1 and 3 km. The internal one, to the northeast consists from peridotite and is of smaller size in the south part of the area of study. In the central to northern part it reaches its largest dimensions, up to a maximum depth of 4 km approximately and a thickness

of 2 km. At the southern part in the area of Vavdos, the internal ophiolitic stripe "fades" out.

The 2.5D joint inversion of the gravity and aeromagnetic data as well as the fact that the profiles along which 2.5D modeling was applied cover a big part of the ophiolitic exposure in the area confirm the robustness of the results of the present work compared to the previous referenced studies. Moreover, the susceptibility values determined both by the inversion procedure as well as by the field measurements from various researchers suggest a similar pattern of strong spatial variation of the susceptibility.

Acknowledgments

We would like to thank Dr. C. Ebinger and an anonymous reviewer for their detailed comments on the manuscript, which helped to improve considerably the present work.

References

Corbato, C.E.: 1965, A least-squares procedure for gravity interpretation, *Geophysics* **30**, 228–233.

Edel, J.B., Kondopoulou, D., Pavlides, S., and Westphall, M.: 1991/1992, Paleomagnetic evidence for a large counterclockwise rotation of northern Greece prior to the Tertiary clockwise rotation, *Geodinamica Acta (Paris)* **5**(4), 245–249.

Jackson, J.A. and McKenzie, D.P.: 1988, The relationship between plate motions and seismic moment tensors, and the rates of active deformation in the Mediterranean and the Middle East, *Geoph. J. R. Astron. Soc.* **93**, 45–73.

Johnson, W.M.: 1969, A least-squares method of interpreting magnetic anomalies caused by two-dimensional structures, *Geophysics* **34**, 65–74.

Kaufman, G., Kockel, F., and Mollat, H.: 1976, Notes on the stratigraphic and paleogeographic position of the Svoula formation in the innermost zone of the Hellenides (Northern Greece), *Bull. Soc. Geol. Fr.* **18**, 225–230.

King, T.A.: 1998, Mechanisms of Isostatic Compensation in Areas of Lithospheric Extension: Examples from the Aegean, Ph.D. Thesis, Univ. of Leeds.

Kiriakidis, L.G.: 1984, Geophysical studies of the Eastern margin of the Vardar Zone in Central Macedonia, Greece, Ph.D. Thesis, Univ. of Cardiff, (UK).

Lagios, E., Chailas, S., Hipkin, R.G., and Drakopoulos, J.: 1994, Gravity and Topographic Data Banks of Greece, University of Athens, Dept. of Geophysics, Public No 4/94, 50 pp.

Lagios, E., Chailas, S., and Hipkin, R.G.: 1995, Gravity and Isostatic Anomaly Maps of Greece Produced, EOS, Transactions, American Geophysical Union, 76/28, 274.

Lagios, E., Chailas, S., and Hipkin, R.G.: 1996, Newly compiled Gravity and Topographic Data Banks of Greece, *Geophysical J. Intern.* **126**, 287–290.

Makris, J. and Moller, L.: 1977, Geophysical studies of the Chalkidiki phiolites and their tectonic implications, *Proc. 6th Coll. of Geology of the Aegean Region*, I.G.M.E. Athens.

Makris, J. and Stavrou, A.: 1984, Compilation of gravity maps of Greece, Hamburg University, Institute of Geophysics.

Mercier, J-L.: 1968, Etude geologique des zones internes des Hellenides en Macedoine centrale. Contribution a l'etude du metamorphism et de l'evolution magmatique des zones internes des Hellenides, *Ann. Geol. Pays Hell.* **20**, 1–792.

Moreli, C., Gantar, G., and Pisani, M.: 1975a, Bathymetry, gravity and magnetism in the strait of Sicily and the Ionian sea, *Boll. Geofis. Teor. Appl.* **17**, 39–58.

Moreli, C., Pisani, M., and Gantar, G.: 1975b, Geophysical studies in the Aegean Sea and in the Eastern Mediterranean, *Boll. Geofis. Teor. Appl.* **18**, 127–167.

Mountrakis, M.D.: 1985, Geology of Greece, Thessaloniki, University Studio Press, (in Greek).

Mountrakis, M,D.: 1990, Geotectonic Evolution of the broader area of Greece, Aristotle University of Thessaloniki, (in Greek).

Papazachos, B.C.: 1990, Seismicity of the Aegean and surrounding area, *Tectonophysics* **178**, 287–308.

Papazachos, C.B.: 1998, Crustal P- and S-velocity of the Serbomacedonian Massif (Northern Greece) obtained by non-linear inversion of traveltimes, *Geophys. J. Int.* **134**, 25–39.

Philipopoulos, N.G.: 1983, A Paleomagnetic and Aeromagnetic Investigation of the Chalkidiki ophiolitic complex, Northern Greece, M. Sc. Thesis, Univ. of Cardiff.

Rasmussen, R. and Pedersen, L.B.: 1979, End corrections in potential field modeling, *Geophysical Prospecting* **27**, 749–760.

Roussos, N.: 1993, The deposit of the gas hydrocarbon of Epanomi (Thessaloniki), An example from a cracked reservoir, *Proc. 6th Congress of the Geol. Soc. of Greece* **2**, 507–523, (in Greek).

Roussos, N.: 1994, Stratigraphy and paleogeographic evolution of the Paleogene Mollasic Basins of the North Aegean Area, *Proc. 7th Congress of the Geol. Soc. of Greece* **2**, 275-294, (in Greek).

Shuey, R.T. and Pasquale, A.S.: 1973, End corrections in magnetic profile interpretation, *Geophysics* **38**, 507–512.

Sousounis, G.: 1993, Estimation of the Hot Dry Rocks resolved of deep boreholes and seismic data, *Proc. 2nd Congress of the Geophysical Soc. of Greece* **2**, 276–287, (in Greek).

Tranos, M.D.: 1998, Contribution to the study of the neotectonic deformation in the region of Central Macedonia and North Aegean, Ph.D. Thesis, Univ. of Thessaloniki (in Greek).

Tranos, M.D., Kilias, A.A., and Mountrakis, D.M.: 1999, Geometry and kinematics of the Tertiary post-metamorphic Circum Rhodope Belt Thrust System (CRBTS), Northern Greece, *Geological Society of Greece* **XXXIII**, 5–16.

Vergely, P.: 1984, Tectonique des ophiolitesdans le Hellenides internes. Consequences sur l'evolution des regions Tethysienns occidentales, These Doct. d'Etat, Paris/Sud.

Webring, M.W.: 1985, SAKI – A FORTRAN program for generalized inversion of gravity and magnetic profiles, *U.S. Geol. Surv. Open-File Rep.*, 85–122.